# IMPACT OF GPU UNCERTAINTY ON THE TRAINING OF PREDICTIVE DEEP NEURAL NETWORKS

**Maciej Pietrowski, Andrzej Gajda**
Faculty of Psychology and Cognitive Sciences
Adam Mickiewicz University
Święty Marcin 78, Poznań 61-809, Poland
maciejpietrowski95@gmail.com,
andrzej.gajda@amu.edu.pl

**Takuto Yamamoto**
Faculty of Medicine
Osaka University
Yamadaoka 1-1, Suita
Osaka, 565-0871, Japan
yam.tak1216@gmail.com

**Taisuke Kobayashi**
Laboratory of Neurophysiology
National Institute for Basic Biology
Higashiyama 5-1, Myodaiji-cho, Okazaki
Aichi, 444-8787, Japan
tkoba@nibb.ac.jp

**Lana Sinapayen**
SONY Computer Science Laboratories
13-1 Hontorocho, Shimogyo Ward
Kyoto 600-8086, Japan
lana.sinapayen@gmail.com

**Eiji Watanabe***
Laboratory of Neurophysiology
National Institute for Basic Biology
Higashiyama 5-1, Myodaiji-cho, Okazaki
Aichi, 444-8787, Japan
eijwat@gmail.com,
eiji@nibb.ac.jp

## ABSTRACT

Deep neural networks often present uncertainties such as hardware- and software-derived noise and randomness. We studied the effects of such uncertainty on learning outcomes, with a particular focus on the function of graphics processing units (GPUs), and found that GPU-induced uncertainty increased learning accuracy of a certain deep neural network. When training a predictive deep neural network using only the CPU without the GPU, the learning error is higher than when training the same number of epochs using the GPU, suggesting that the GPU plays a different role in the learning process than just increasing the computational speed. Because this effect cannot be observed in learning by a simple autoencoder, it could be a phenomenon specific to certain types of neural networks. GPU-specific computational processing is more indeterminate than that by CPUs, and hardware-derived uncertainties, which are often considered obstacles that need to be eliminated, might, in some cases, be successfully incorporated into the training of deep neural networks. Moreover, such uncertainties might be interesting phenomena to consider in brain-related computational processing, which comprises a large mass of uncertain signals.

## 1 INTRODUCTION

Large systems often present uncertainties such as hardware- and software-derived noise and randomness, which designers do not prefer. Deep neural networks, which have recently been used in the development of artificial intelligence (AI), are no exception. The randomness associated with the initial node-weight values and the nondeterminism of computational processes involving graphics

*also affiliated to Department of Basic Biology, The Graduate University for Advanced Studies (SOKENDAI), Miura, Kanagawa 240-0193

processing units (GPUs) (Nagarajan et al., 2018) (e.g., float operations (Morin & Willetts, 2020) and matrix computations when optimizing computational speed (Pham et al., 2020)) are related to the uncertainty of training results from deep neural networks and often destabilize the learning results and hinder reproducibility. However, uncertainty does not have only negative effects on learning outcomes. For example, the dropout method randomly introduces unlearned nodes during the training process while suppressing overfitting during network learning (Srivastava et al., 2014). Alternatively, randomly initialized feed-forward networks can be used for efficient learning by neural networks Frankle & Carbin (2018). Although a theoretical understanding of the effects of uncertainty has not been achieved, investigating the effect of uncertainty on neural networks is beneficial for further development of AI. Therefore, in this study, we investigated the effect of uncertainty, with a specific focus on uncertainties associated with GPU processing, on network training using an autoencoder (Hinton & Salakhutdinov, 2006) and predictive deep neural networks (PredNet, Lotter et al. (2017)).

## 2 METHODS

### 2.1 TRAINING

An autoencoder and PredNet were used in this study (Supplemental Figure 1: Fig. 9), with both networks trained using an image dataset. After training, the networks output appropriate images (y) against input images (x). The labeling data associated with the images were not used for training, i.e., unsupervised learning was used. For the autoencoder, the training progressed such that one image was input, followed by output of the exact same image. For the PredNet, a sequential video image was used as input, followed by learning and subsequent output of an image relative to the input image. PredNet is based on a hypothesis used to explain the operation of the cerebral cortex (predictive coding, Rao & Ballard (1999)). The neural network trained for prediction emulates the diverse features of biological neurons (Lotter et al., 2020) and perception, including visual illusions (Watanabe et al., 2018; Lotter et al., 2020). The autoencoder and PredNet were both written in Chainer (Tokui et al., 2015) and embedded into interface code (`https://doi.org/10.6084/m9.figshare.12318953` and `https://doi.org/10.6084/m9.figshare.5483710`, respectively) that was also used in a previous experiment (Watanabe et al., 2018). The autoencoder was trained using the Modified National Institute of Standards and Technology (MNIST) dataset comprising handwritten digits (LeCun & Cortes, 2010). A single image ($224 \times 224$ pixels, Supplemental Figure 2: Fig. 10] was backpropagated as a single batch, with a total of 5000 batches performed for training using 5000 images. PredNet was trained with the first-person social interactions (FPSI) dataset (Fathi et al., 2012), which contains day-long self-view motion videos of subjects at the Disney World Resort in Orlando, Florida. Image size was $160 \times 120$ pixels (Supplemental Figure 3: Fig. 11). Twenty consecutive images were backpropagated as a single batch, with 250 training batches prepared using 5000 images. We applied four learning conditions that varied according to the different settings used in the cuDNN functions (Chetlur et al., 2014) and the initial values for the node weights. cuDNN functions are Python libraries used to optimize the computational speed of GPUs, and initial node-weight values denote the first value of weight data assigned to a given network. The conditions were as follows: 1) cuDNN functions were turned on, and initial values were randomly selected; 2) cuDNN functions were turned off ("export CHAINER_CUDNN=0"), and initial values were randomly selected; 3) cuDNN functions were turned on, and initial values were fixed (one value was derived from training using condition 1; autoencoder model: `https://doi.org/10.6084/m9.figshare.12318953`; PredNet model: `https://doi.org/10.6084/m9.figshare.12318950`); and 4) cuDNN functions were turned off, and initial values were fixed. The networks were trained with the mean-squared error of the first layer, and neither the autoencoder nor the PredNet used the dropout process. All program codes (autoencoder: `https://doi.org/10.6084/m9.figshare.12318953`; and PredNet: `https://doi.org/10.6084/m9.figshare.5483710`) and datasets (autoencoder: `https://doi.org/10.6084/m9.figshare.12318953`; PredNet: `https://doi.org/10.6084/m9.figshare.5483668`) are available at Figshare (`https://figshare.com`).

### 2.2 Hardware

Training was performed on CPUs without GPUs (Intel i5-4590, i7-6800K, i5-7600K, or AMD Ryzen-5-3600) or CPUs with GPUs (Intel i5-7600K + NVIDIA GTX-750Ti, i5-7600K + GTX-970, i7-6700K + GTX-1080, i7-7700K + GTX-1080Ti, i7-9700 + RTX-2080Ti, i5-7600K + RTX-2060 super, AMD Ryzen-5-3600 + RTX-2070 super, or i5-9400 + Titan-RTX). In the absence of GPUs, we used htop (`https://hisham.hm/htop/`), an interactive process viewer for Unix systems, to ensure that training was performed on a single thread (Intel i7-6800K), four threads (Intel i5-4590 and i5-7600K), or six threads (AMD Ryzen-5-3600).

### 2.3 Model Generalisability

The generalization of the trained PredNet was analyzed against 12 static images (Supplemental Figure 4: Fig. 12) randomly selected from the Moments in Time (MIT) dataset (Monfort et al., 2019). Twenty consecutive copies of the same image were used as input for the models, and the loss value (mean-squared error) for the predicted image for the 20th input image was analyzed. Loss values against 12 static images were averaged. Generalization performance was calculated using the GTX-1080Ti GPU with the cuDNN functions turned off.

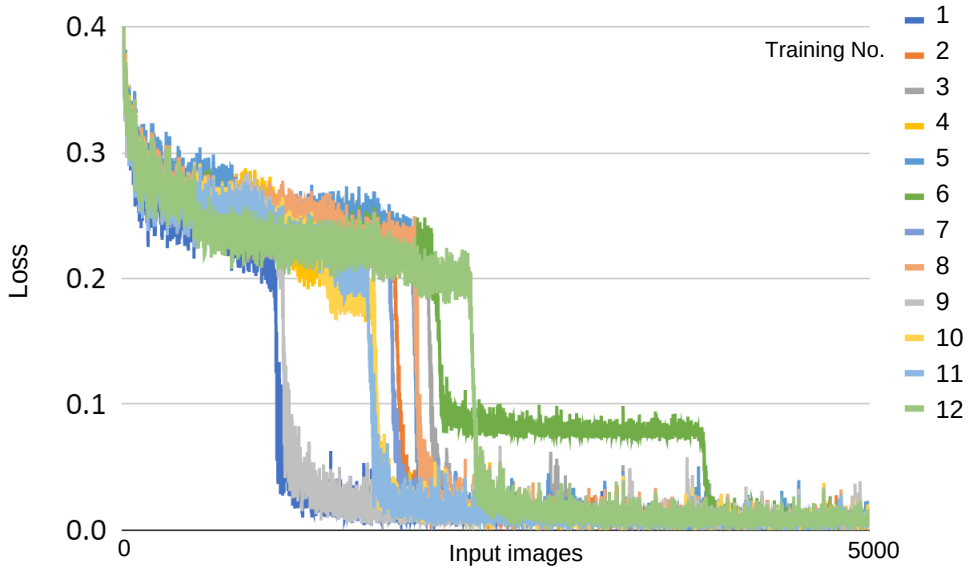


Figure 1: Learning curves for the autoencoder using 12 randomly selected initial values. The vertical axis represents the loss value, and the horizontal axis represents the number of images (1 image = 1 batch). Twelve rounds of training were performed under condition 1 (cuDNN = on, initial values = random) on a 1080Ti GPU.

## 3 Results

### 3.1 Autoencoder performance

We first evaluated the effects of initial values for node weight and the status of the cuDNN functions using the autoencoder and the MNIST dataset (Supplemental Figure 1: Fig. 10). Fig. 1 shows the learning curves generated from 12 different randomly selected initial values, revealing similar curves but different timings for their escape from the saddle point. Eleven of the 12 trials resulted in biphasic learning curves, whereas only one resulted in a triphasic curve, suggesting that there were multiple different saddle points. To assess the differences in the final learning results, we averaged the loss values of the final 50 batches of learning among the 5000 training batches (Fig. 2-a), revealing a mean ± standard deviation of $0.0074 \pm 0.00074$ for the 12 values. A similar result was

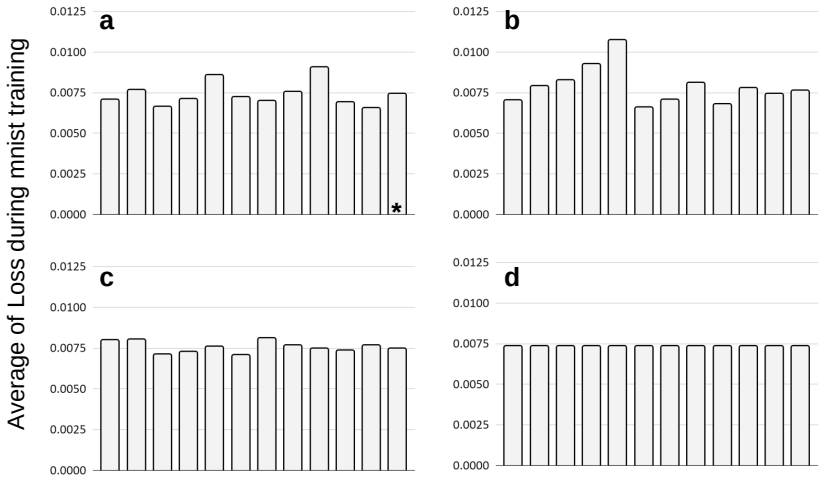


Figure 2: Average loss from the autoencoder during training with the MNIST dataset under four different conditions. A total of 5000 images (5000 batches) were trained, with an average loss value for the final 50 images (50 batches) shown. The training was conducted 12 times for each condition. (a–d) Models trained under conditions 1–4. The initial model used for conditions 3 and 4 was the same as that used for the 12th round of training (asterisk) for condition 1. All training rounds were performed using a 1080Ti GPU. (d) Training was conducted using the same initial values and the same GPU with cuDNN functions turned off, resulting in identical average loss values.

obtained when cuDNN functions were turned off ($0.0079 \pm 0.0012$; Fig. 2-b). Even under conditions involving a fixed initial value, a similar variation was maintained when the cuDNN functions were turned on ($0.0076 \pm 0.00035$; Fig. 2-c). The results suggested that the variation observed from the training conditions was a mixed effect of randomized initial values and the cuDNN functions. When the initial value was fixed and the cuDNN functions were turned off, the results of the 12 training sessions were identical ($0.0073 \pm 0$; Fig. 2-d).

We then evaluated the effects of hardware architecture on uncertainty in the training results. The experiments were conducted under various hardware architectures using condition 4 to eliminate software-related uncertainty. Fig. 3 shows the results derived from four different CPUs and eight GPUs. We observed relatively small variations ($0.0075 \pm 0.00020$) for all 12 architectures; however, there was evidence of learning indeterminacy. The mean difference between CPUs and GPUs was small (CPUs: $0.0076 \pm 0.00023$; and GPUs, $0.0074 \pm 0.00017$).

### 3.2 Predictive deep neural network performance

We assessed PredNet trained with the FPSI dataset. PredNet is capable of learning highly complex video input compared with the autoencoder. Fig. 4 shows the learning curves generated from 12 different randomly selected initial values and that the amount of loss significantly fluctuated relative to that observed using the autoencoder. This was likely (in part at least) due to the input data being first-person video from a motion camera, which resulted in a lot of switching between scenes. As with the autoencoder, the timing of the escape from the saddle point differed among the 12 training sessions. We then performed experiments under various conditions (1–4), which resulted in similar mean values for each of the 12 initial values (condition 1: $0.012 \pm 0.00077$; condition 2: $0.012 \pm 0.0013$; condition 3: $0.011 \pm 0.00011$; and condition 4: $0.011 \pm 0$)(Fig. 5). Both the initial values and cuDNN status affected the loss value, although the initial values had a stronger effect.

We then observed characteristic hardware dependence (Fig. 6). Notably, training on GPUs resulted in lower losses as learning progressed, which was not observed when training using CPUs without GPUs ($0.033 \pm 0.032$ for use with GPU and CPU combinations; $0.077 \pm 0.000022$ for use with CPUs alone; and $0.011 \pm 0.00019$ for use with GPUs alone). There was little difference among the GPUs. There was also little difference among the CPUs.

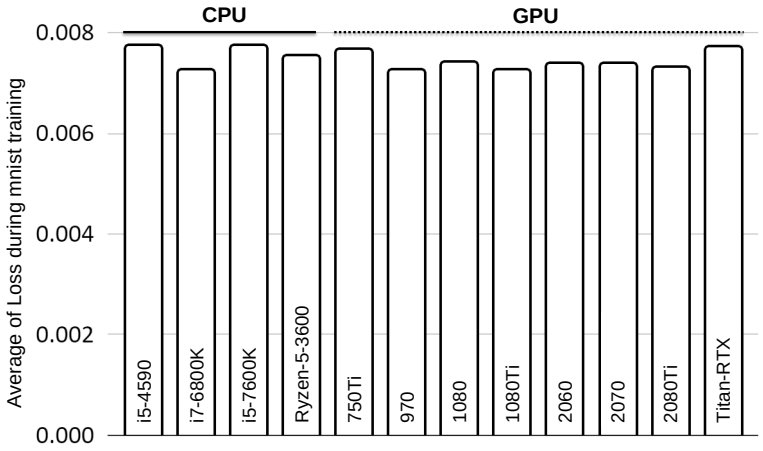


Figure 3: Average loss from the autoencoder during training with the MNIST dataset using four CPUs and eight GPUs. A total of 5000 images (5000 batches) were used for training, with the average loss values for the final 50 images (50 batches) shown. The training conditions were the same as those described in Fig. 2-d (cuDNN = off; initial value = fixed).

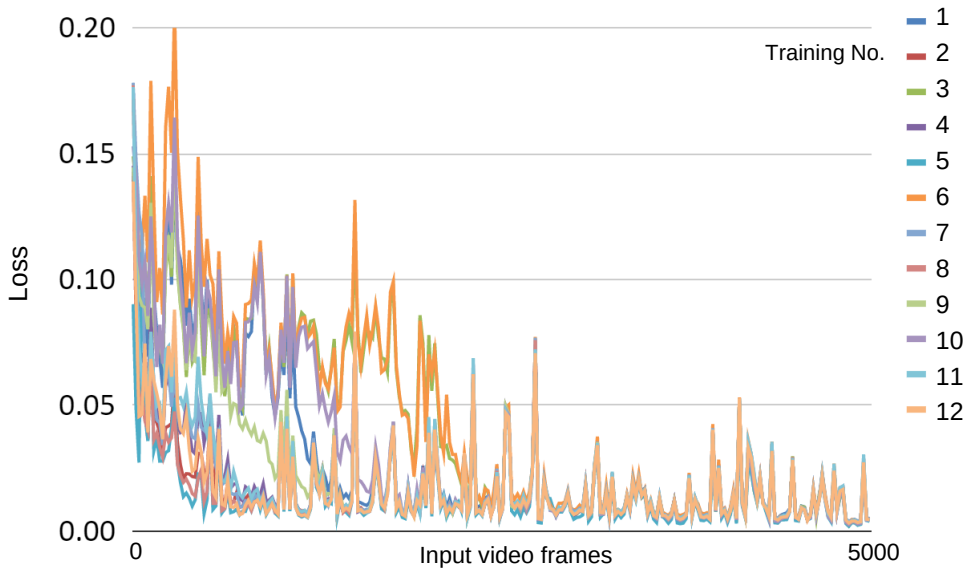


Figure 4: Learning curves generated for the PredNet using 12 randomly selected initial values. The vertical axis represents loss value, and the horizontal axis represents the number of video frames (1 batch = 20 frames). Twelve rounds of training were performed under condition 1 (cuDNN = on; initial value = random). All training rounds were performed on a 1080Ti GPU.

PredNet trained using the self-motion video accurately reproduced an extremely wide range of images. Therefore, we investigated the generalized performance of PredNet models in more detail using 12 still images from the MIT dataset (Supplemental Figure 4: Fig. 12). The PredNet model used was that obtained from the 5000-video-frame training (Fig. 5) and resulted in similar average losses under each condition (condition 1: $0.011 \pm 0.0033$; condition 2: $0.012 \pm 0.0037$; condition 3: $0.0058 \pm 0.00012$; and condition 4: $0.0060 \pm 0$)(Figs. 7, Supplemental Figure 5: Fig. 13). The results showed that low loss values during training did not necessarily represent high generalized performance. Furthermore, both the initial values and cuDNN status affected the loss variance, with

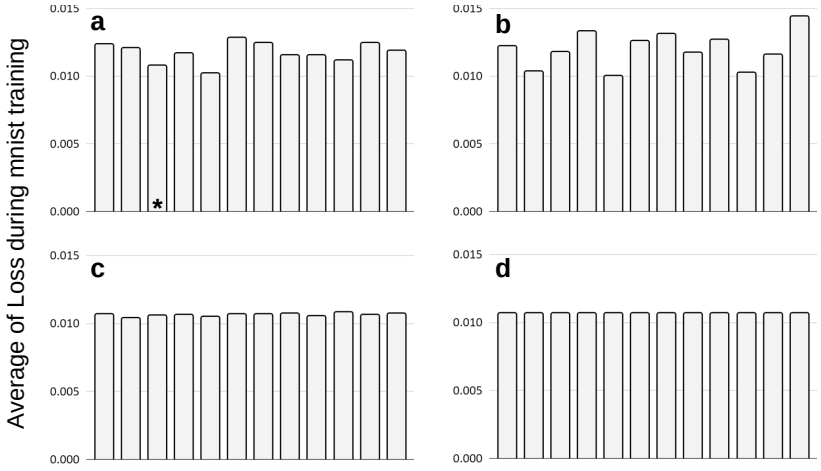


Figure 5: Average loss by the PredNet during FPSI training under four different conditions. A total of 5000 video frames (250 batches) were used for training, with the average loss value for the final 1000 video frames (50 batches) shown. The training was conducted 12 times for each condition. (a–d) Models trained under conditions 1–4. The initial model used in conditions 3 and 4 was the same as that used for the 3rd round of training (asterisk) under condition 1. All training iterations were performed on a 1080Ti GPU. (d) Training using the same initial values and the same GPU with cuDNN functions turned off resulted in the exact same average loss values.

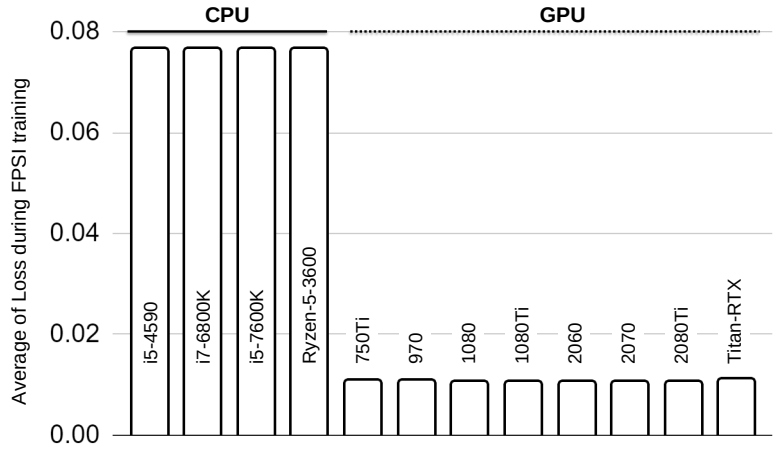


Figure 6: Average loss by PredNet during FPSI training using four CPUs and eight GPUs. The network was trained on a total of 5000 video frames (250 batches), with the average loss for the final 1000 video frames (50 batches) shown. The training conditions were the same as those described in Fig. 5-d (condition 4: cuDNN = off; initial value = fixed). The training results differed substantially between CPU and GPU.

the initial values having a stronger effect, and the generalized performance of the model obtained using a CPU was significantly worse than that using a GPU ($0.030 \pm 0.035$ using GPU and CPU combinations with 250-batch training; $0.077 \pm 0.00095$ using CPUs alone; and $0.0058 \pm 0.00019$ using GPUs alone) (Fig. 8, Supplemental Figure 6: Fig. 14). Evaluation of training progress from input video frames 2000-5000 (batches 50–250) revealed that the CPU-based training showed a slight improvement in performance, where this improvement was lower than that observed in GPU-based training (Fig. 8).

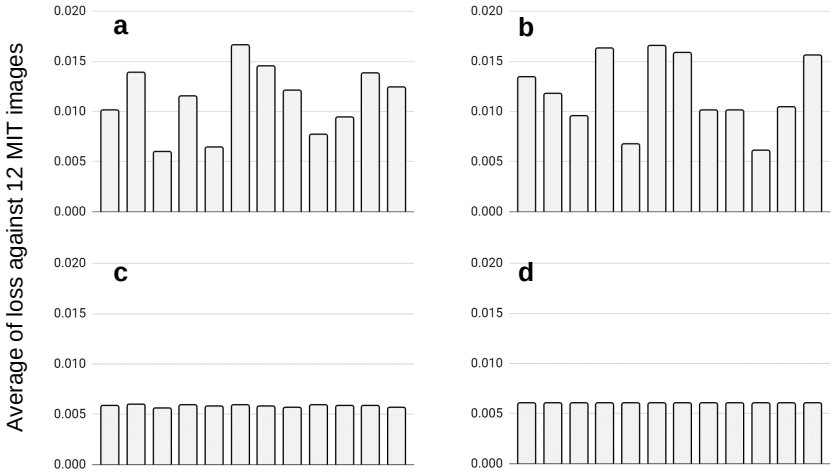


Figure 7: Generalized performance of the PredNet using models trained under four different conditions. (a–d) Models trained under conditions 1–4. The fixed initial value was the same as that used during the 3rd round of training under condition 1 (asterisk in Fig. 5). All training iterations were performed using a 1080Ti GPU. The trained models used were the same as those trained using 5000 video frames (Fig. 5). The vertical axis represents the average predicted loss for the 12 images.

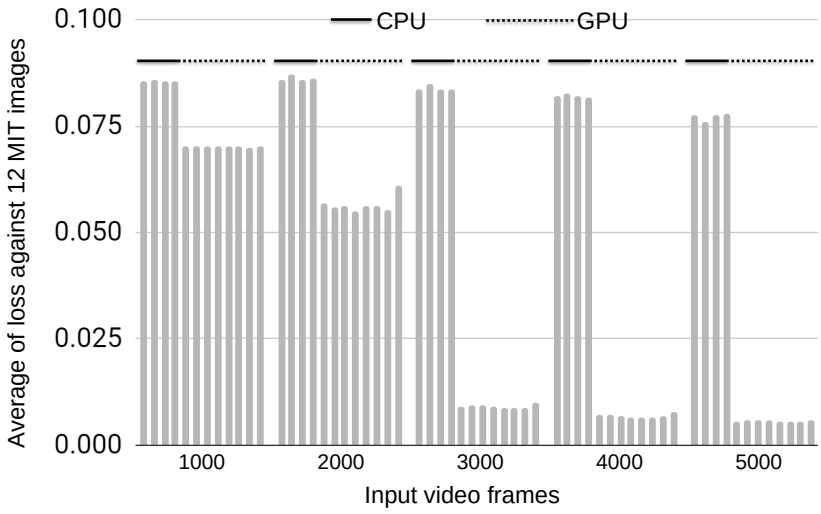


Figure 8: Generalized performance of the PredNet during FPSI training using four CPUs and eight GPUs. PredNet was trained under condition 4 (cuDNN = off; initial value = fixed) using 12 different hardware configurations, and generalized performance was measured after every 1000 input video frames. The vertical axis represents the average predictive loss for 12 images. The order of the hardware is the same as in Fig. 6. Learning did not proceed rapidly using a CPU.

## 4 Discussion

The current experiments showed that initial values, cuDNN, and hardware were involved in the variability of DNN training results. Variations due to hardware were observed in the training of the two DNNs, especially in PredNet, where large differences were observed between CPU and GPU. Although the mechanism is unclear, the GPU hardware seems to have the ability to advance the training of DNNs.

### 4.1 AUTOENCODER AND PREDNET

Both the autoencoder and PredNet are DNNs that generate appropriate images through unsupervised learning (Hinton & Salakhutdinov, 2006; Lotter et al., 2017). However, the network structure of the two is completely different: Autoencoder learns simple still image data to generate still images, while PredNet learns complex video data to generate predictive images. Despite the large difference in the nature of the two, it should be noted that the initial value, cudnn, and hardware had an equal effect on the variability of the learning results for both.

### 4.2 UNCERTAINTY AND DEEP NEURAL NETWORKS

In deep learning papers, stationary points such as local maxima, local minima, and saddle points have been considered to be not a big problem by many practitioners since a long time ago. It has been partially proven theoretically. Kawaguchi proved that local minima should not be a problem for the squared loss function of deep linear neural networks with any depth and any width (Kawaguchi, 2016). However, the paper pointed out that we should continue to pay attention to the saddle points. In order to avoid learning suppression by the saddle points, various methods related to stochastic gradient descent (SGD) have been introduced into deep learning. Allen-Zhu et al. argued that SGD can find global minima on the training objective of DNNs in polynomial time, assuming that the input is non-degenerate and the network is over-parameterized (Allen-Zhu et al., 2019). The paper suggested that the randomness of SGD allows deep neural networks to successfully avoid saddle points. However, as shown in this experiment without SDG (e.g., Fig. 6), it seems that SDG is not the only tool that can help avoid saddle points. Uncertainty in GPUs may also act as a tool for avoiding saddle points, although we have not been able to know this until now because neural networks are rarely studied on CPUs (Mittal et al., 2021).

## REFERENCES


Zeyuan Allen-Zhu, Yuanzhi Li, and Zhao Song. A convergence theory for deep learning via over-parameterization. In *International Conference on Machine Learning*, pp. 242–252. PMLR, 2019.

Sharan Chetlur, Cliff Woolley, Philippe Vandermersch, Jonathan Cohen, John Tran, Bryan Catanzaro, and Evan Shelhamer. cudnn: Efficient primitives for deep learning. *CoRR*, abs/1410.0759, 2014. URL http://arxiv.org/abs/1410.0759.

Alircza Fathi, Jessica K Hodgins, and James M Rehg. Social interactions: A first-person perspective. In *2012 IEEE Conference on Computer Vision and Pattern Recognition*, pp. 1226–1233. IEEE, 2012.

Jonathan Frankle and Michael Carbin. The lottery ticket hypothesis: Training pruned neural networks. *CoRR*, abs/1803.03635, 2018. URL http://arxiv.org/abs/1803.03635.

Geoffrey E Hinton and Ruslan R Salakhutdinov. Reducing the dimensionality of data with neural networks. *Science*, 313(5786):504–507, 2006.

Kenji Kawaguchi. Deep learning without poor local minima, 2016. URL https://arxiv.org/abs/1605.07110.

Yann LeCun and Corinna Cortes. MNIST handwritten digit database. 2010. URL http://yann.lecun.com/exdb/mnist/.

William Lotter, Gabriel Kreiman, and David D. Cox. Deep predictive coding networks for video prediction and unsupervised learning. *CoRR*, abs/1605.08104, 2017. URL http://arxiv.org/abs/1605.08104.

William Lotter, Gabriel Kreiman, and David Cox. A neural network trained for prediction mimics diverse features of biological neurons and perception. *Nature Machine Intelligence*, 2(4):210–219, 2020.

Sparsh Mittal, Poonam Rajput, and Sreenivas Subramoney. A survey of deep learning on cpus: Opportunities and co-optimizations. *IEEE Transactions on Neural Networks and Learning Systems*, pp. 1–21, 2021. doi: 10.1109/TNNLS.2021.3071762.

Mathew Monfort, Alex Andonian, Bolei Zhou, Kandan Ramakrishnan, Sarah Adel Bargal, Tom Yan, Lisa Brown, Quanfu Fan, Dan Gutfruend, Carl Vondrick, et al. Moments in time dataset: one million videos for event understanding. *IEEE Transactions on Pattern Analysis and Machine Intelligence*, pp. 1–8, 2019. ISSN 0162-8828. doi: 10.1109/TPAMI.2019.2901464.

Miguel Morin and Matthew Willetts. Non-determinism in tensorflow resnets. *CoRR*, abs/2001.11396, 2020. URL `https://arxiv.org/abs/2001.11396`.

Prabhat Nagarajan, Garrett Warnell, and Peter Stone. The impact of nondeterminism on reproducibility in deep reinforcement learning. 2018. URL `https://arxiv.org/abs/1809.05676`.

Hung Viet Pham, Shangshu Qian, Jiannan Wang, Thibaud Lutellier, Jonathan Rosenthal, Lin Tan, Yaoliang Yu, and Nachiappan Nagappan. Problems and opportunities in training deep learning software systems: An analysis of variance. In *2020 35th IEEE/ACM International Conference on Automated Software Engineering (ASE)*, pp. 771–783, 2020.

Rajesh PN Rao and Dana H Ballard. Predictive coding in the visual cortex: a functional interpretation of some extra-classical receptive-field effects. *Nature neuroscience*, 2(1):79–87, 1999.

Nitish Srivastava, Geoffrey Hinton, Alex Krizhevsky, Ilya Sutskever, and Ruslan Salakhutdinov. Dropout: a simple way to prevent neural networks from overfitting. *The journal of machine learning research*, 15(1):1929–1958, 2014.

Seiya Tokui, Kenta Oono, Shohei Hido, and Justin Clayton. Chainer: a next-generation open source framework for deep learning. In *Proceedings of workshop on machine learning systems (LearningSys) in the twenty-ninth annual conference on neural information processing systems (NIPS)*, volume 5, pp. 1–6, 2015.

Eiji Watanabe, Akiyoshi Kitaoka, Kiwako Sakamoto, Masaki Yasugi, and Kenta Tanaka. Illusory motion reproduced by deep neural networks trained for prediction. *Frontiers in psychology*, 9: 345, 2018.

# A APPENDIX

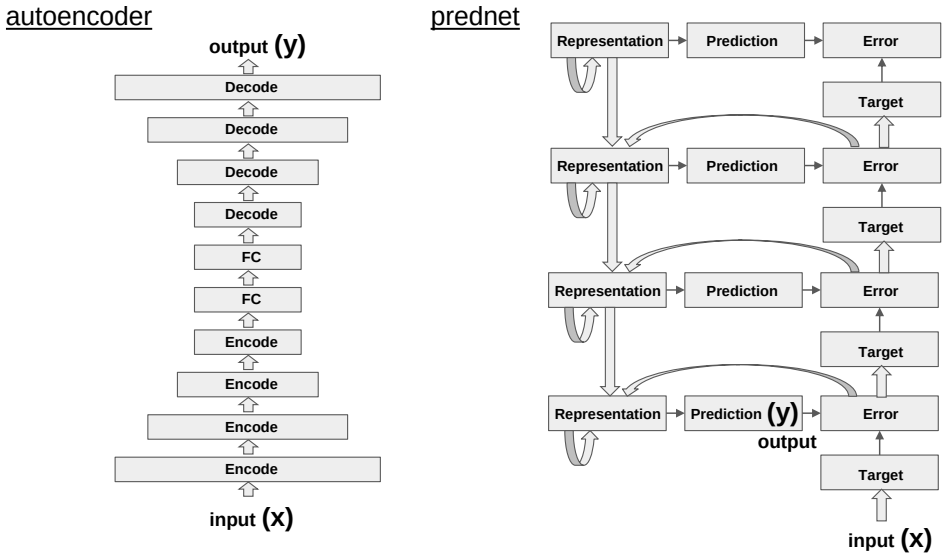


Figure 9: [Supplemental Figure 1] Autoencoder and predictive coding network (PredNet). Information flow within a 10-layer autoencoder (left). An autoencoder comprises three parts: the encoder (Encode, convolution layers), hidden units [fully connected layers], and the decoder (Decode, convolution layers). Its purpose is to reconstruct inputs rather than predict a target value, y, given input x. Illustration of information flow within four layers of PredNet (right). Each layer comprises representation neurons (Representation, convolutional long short-term memory) that output a layer-specific prediction (Prediction) at each time step, which is then compared with a target (Target) to produce an error term (Error) that propagates laterally and vertically in the network. The PredNet has recurrent flows of information within and across the layers and learns to minimize the difference between the Prediction and Target of the lowermost layer. The autoencoder and PredNet are unsupervised-learning models.

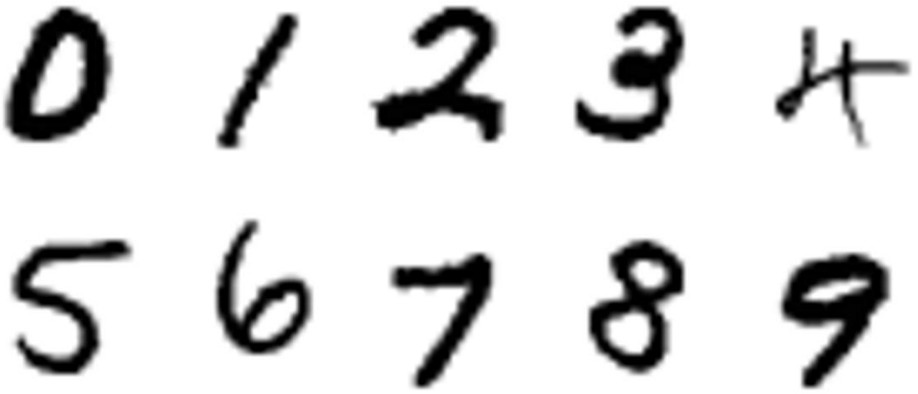

Figure 10: [Supplemental Figure 2] Samples of the Modified National Institute of Standards and Technology (MNIST) dataset used for the autoencoder experiments. The MNIST database includes handwritten digits, where black and white images are normalized to fit into a $28 \times 28$ pixel bounding box and anti-aliased to introduce grayscale levels. The database contains 60,000 training images and 10,000 test images.


Figure 11: [Supplemental Figure 3] Samples of the first-person social interactions (FPSI) dataset. The FPSI dataset contains day-long videos of eight subjects spending their day at Disney World Resort in Orlando, Florida. The cameras were mounted on a cap worn by one of the subjects. Five consecutive frames of images are shown in time sequence for three portions of the video.

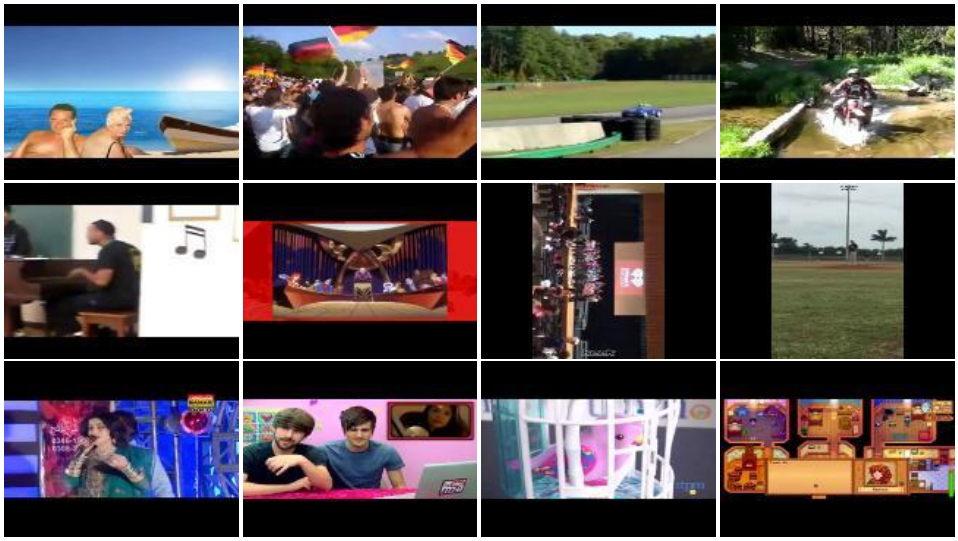

Figure 12: [Supplemental Figure 4] Test images from the MIT dataset used to assess the generalized performance of the PredNet. The MIT dataset includes a collection of 1 million labeled 3-second videos involving people, animals, objects, or natural phenomena that capture a dynamic scene. Twelve images were randomly selected.

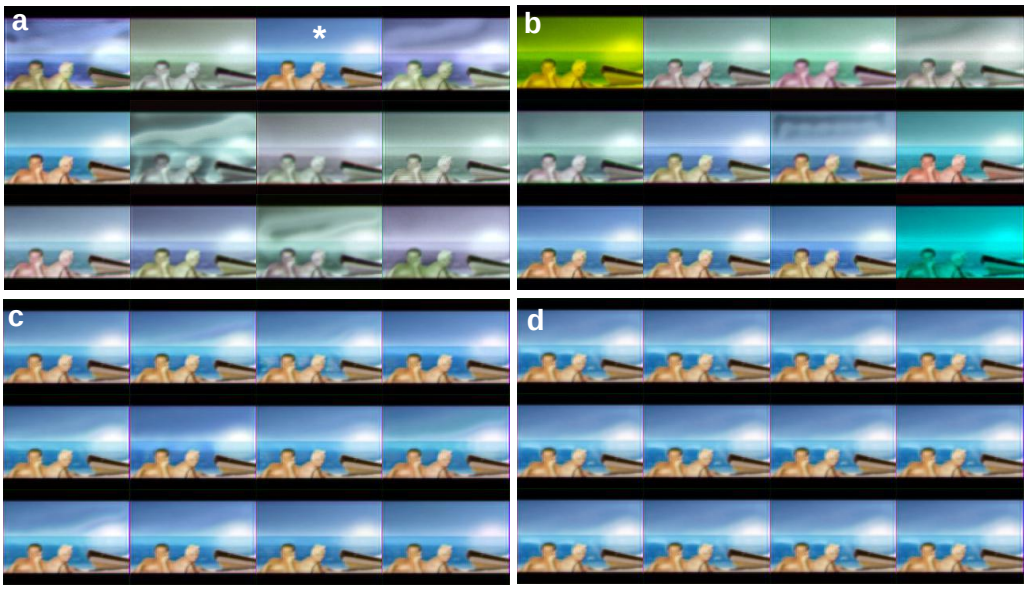


Figure 13: [Supplemental Figure 5] Generalized performance. Images predicted from one sample image. (a–d) Models trained under conditions 1–4. The fixed initial value was the same as that used in the 3rd round of training under condition 1 (asterisk). All training iterations were performed using a 1080Ti GPU.

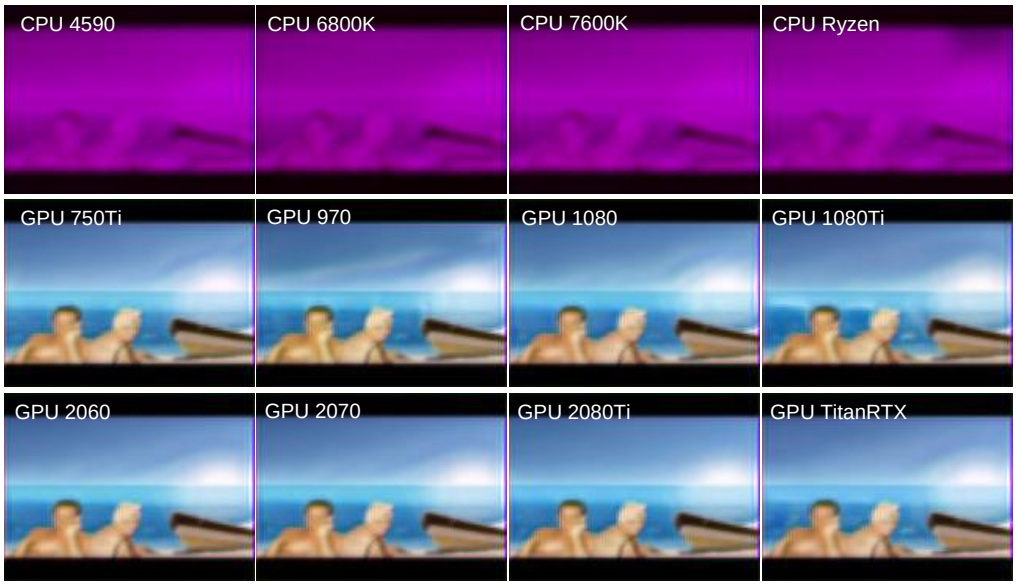


Figure 14: [Supplemental Figure 6] Generalized performance using 12 different hardware configurations. The image used and training condition (condition 4) were the same as those described in Fig. 7. The model underwent 5000 video frames (250-batch) training. Models trained using the CPU demonstrated poor image prediction.